PHYSICAL REVIEW D **93,** 093011 (2016)

Dark-photon searches via Higgs-boson production at the LHC

Sanjoy Biswas,[1] Emidio Gabrielli,[2,3] Matti Heikinheimo,[4] and Barbara Mele[5]

[1]*KIAS, 85 Hoegi-ro, Dongdaemun-gu, Seoul 130-722, Republic of Korea*

[2]*Dipart. di Fisica Teorica, Università di Trieste, Strada Costiera 11, I-34151 Trieste, Italy and INFN, Sezione di Trieste, Via Valerio 2, I-34127 Trieste, Italy*

[3]*NICPB, Ravala 10, 10143 Tallinn, Estonia*

[4]*Helsinki Institute of Physics, University of Helsinki, P.O.Box 64, FI-00014 Helsinki, Finland*

[5]*INFN, Sezione di Roma, P. le A. Moro 2, I-00185 Rome, Italy*

(Received 9 March 2016; published 16 May 2016)

Dark photons $\bar{\gamma}$ mediating long-range forces in a dark sector are predicted by various new physics scenarios, and are being intensively searched for in experiments. We extend a previous study of a new discovery process for dark photons proceeding via Higgs-boson production at the LHC. Thanks to the nondecoupling properties of the Higgs boson, $\mathrm{BR}(H \to \gamma\bar{\gamma})$ values up to a few percent are possible for a massless dark photon, even for heavy dark-sector scenarios. The corresponding signature consists (for a Higgs boson at rest) of a striking monochromatic photon with energy $E_\gamma = m_H/2$, and a similar amount of missing energy. We perform a model-independent analysis at the LHC of both the gluon-fusion and vector-boson fusion (VBF) Higgs production mechanisms at 14 TeV, including parton-shower effects, and updating our previous parton-level analysis at 8 TeV in the gluon-fusion channel by a more realistic background modeling. We find that a 5σ sensitivity can be reached in the gluon-fusion channel for $\mathrm{BR}(H \to \gamma\bar{\gamma}) \simeq 0.1\%$ with an integrated luminosity of $L \simeq 300$ fb^{-1}. The corresponding VBF reach is instead restricted to 1%. Such decay rates can be naturally obtained in dark-photon scenarios arising from unbroken $U(1)_F$ models explaining the origin and hierarchy of the Yukawa couplings, strongly motivating the search for this exotic Higgs decay at the LHC.

DOI: 10.1103/PhysRevD.93.093011

I. INTRODUCTION

Although long awaited, no conclusive signal of new physics (NP) at the TeV scale showed up in the first run of the LHC at 7 and 8 TeV, or in the initial phase of Run 2 at 13 TeV either. As a consequence, consent is growing up around the idea that a new and unexplored *dark* (or *hidden*) sector, weakly coupled to the standard model (SM), is responsible for the observed dark matter (DM). The latter, which is 5 times more abundant in the Universe than ordinary baryonic matter [1], remains still a mystery, with its constituents and detailed properties yet unknown. A dark sector could then have its internal structure and interactions, in complete agreement with present astroparticle and cosmological observations.

It is also conceivable that a hidden sector could contain an extra long-range force mediator among the dark particles. The most simple example is provided by a new unbroken $U(1)$ gauge group, predicting a dark (or hidden) photon in its spectrum [2]. Dark-photon scenarios have been extensively considered in the literature in the framework of NP extensions of the SM gauge group [3–7].

In cosmology, dark photons may help to solve the small-scale structure formation problems. Massless dark photons interacting with dark matter [8] can lead to the formation of dark discs of galaxies [9], analogously to the galaxy structure formation in the ordinary Universe, or to the collisional behavior of dark matter in mergers of galaxies and galaxy clusters [10]. In astroparticle physics, dark photons may induce the Sommerfeld enhancement of the DM annihilation cross section needed to explain the PAMELA-Fermi-AMS2 positron anomaly [11], as well as assist light-DM annihilations to make asymmetric DM scenarios phenomenologically viable [12]. In some scenarios, massive dark photons have also been considered as potential dark-matter candidates, with dedicated experiments looking for their direct detection in the mass range from a few eV up to 100 keV [2,13].

Most present astrophysical and accelerator constraints [2] apply to *massive* dark photons, and can be evaded in the case of a *massless* dark-photon scenario, allowing for potentially large dark-photon couplings in the dark sector. Indeed, in the massless case, *on-shell* dark photons can be fully decoupled from the SM quark and lepton sector [3], which is not true for the massive case due to the potential tree-level mixing with ordinary photons of massive dark photons. This property can lead to observable new signatures at colliders for massless dark photons, provided there is a messenger sector letting the SM and dark sector communicate. Here we will treat the dark photon as a purely massless gauge boson of an unbroken U(1) interaction, and as such it is completely stable. Furthermore, we will assume that at tree-level there is no kinetic mixing with the SM photon. With these assumptions, the dark photon evades most experimental constraints that apply to massive

dark photons with kinetic mixing, as for the scenario described below.

Recently, a massless dark photon scenario has been foreseen in the framework of a theoretical proposal aimed to naturally solve the flavor hierarchy problem [14]. This model predicts a new Higgs-boson decay channel into a photon (γ) and a massless dark-photon ($\bar{\gamma}$)

$$H \to \gamma\bar{\gamma}, \tag{1}$$

which is induced at one loop. The final $\bar{\gamma}$ gives rise to missing energy and momentum in the detector, leading to an exotic resonant monophoton signature at the LHC. The latter features a distinctive photon transverse-momentum (p_T^γ) distribution peaked around $m_H/2$, the same for the missing transverse-energy ($\not{E}_T$) distribution, and a $\gamma\bar{\gamma}$ transverse-mass distribution peaked around m_H. This exotic signature has been recently analyzed for the first time in Ref. [15], in a model-independent way. In particular, a parton-level analysis at the 8 TeV LHC has been performed for the main Higgs-boson production channel, namely the gluon-fusion process. Using the full 8 TeV LHC data set, a 5σ sensitivity for a Higgs $H \to \gamma\bar{\gamma}$ branching ratio (BR) down to 0.5% has been obtained. These results have been worked out under assumptions that might underestimate one of the main reducible backgrounds, given by a photon plus jet (j), and did not include parton-shower effects.

The purpose of the present paper is twofold. On the one hand, we upgrade our previous 8 TeV analysis of the $H \to \gamma\bar{\gamma}$ decay in the main Higgs production channel [15] by adding parton-shower effects to the previous parton-level Monte Carlo study of the signal and of SM backgrounds. We also consider a more realistic background modeling, based on recent experimental studies of events with a photon plus missing energy at the LHC [16]. We then extend the analysis to the upgraded *nominal* LHC energy of 14 TeV. On the other hand, we analyze for the first time an alternative signature coming from the $H \to \gamma\bar{\gamma}$ decay for a Higgs boson produced via the vector-boson fusion (VBF) mechanism. The gluon-fusion channel will turn out to be the most sensitive to $\mathrm{BR}(H \to \gamma\bar{\gamma})$ ($\mathrm{BR}_{\gamma\bar{\gamma}}$). Nevertheless, we will see that the VBF process could significantly contribute to either a measurement or a determination of upper bounds of the decay rate of the exotic Higgs decay into a dark photon, possibly giving an independent confirmation of the signal in case of a positive observation in the gluon-fusion process.

The plan of the paper is the following. In Sec. II, we describe a theoretical framework that might give rise to the $H \to \gamma\bar{\gamma}$ signature with observable rates. In Sec. III A, we study the potential of the gluon-fusion Higgs production mechanism at the LHC for constraining the $H \to \gamma\bar{\gamma}$ rate, by a detailed analysis of both the signal and main backgrounds. The same is done for the VBF production mechanism in Sec. III B. In Sec. IV, we summarize our results and conclude.

II. THEORETICAL FRAMEWORK

We now provide a model-independent parametrization of the amplitude for the $H \to \gamma\bar{\gamma}$ channel, and then discuss the corresponding BR's range that can be expected in a class of NP models that might explain the origin and hierarchy of the Higgs Yukawa couplings.

The $H \to \gamma\bar{\gamma}$ amplitude can be parametrized in a model-independent way by requiring gauge invariance, as follows:

$$M_{\gamma\bar{\gamma}} = \frac{1}{\Lambda_{\gamma\bar{\gamma}}} T_{\mu\nu}(k_1, k_2)\varepsilon_1^\mu(k_1)\varepsilon_2^\nu(k_2), \tag{2}$$

where $\Lambda_{\gamma\bar{\gamma}}$ is the effective scale associated to the NP, $T^{\mu\nu}(k_1, k_2) \equiv g^{\mu\nu} k_1 \cdot k_2 - k_2^\mu k_1^\nu$, and $\varepsilon_1^\mu(k_1)$ and $\varepsilon_1^\mu(k_1)$ are the photon and dark-photon polarization vectors, respectively. The corresponding decay width is given by

$$\Gamma(H \to \gamma\bar{\gamma}) = m_H^3/(32\pi\Lambda_{\gamma\bar{\gamma}}^2). \tag{3}$$

A massless dark photon does not couple to SM particles at tree level. One can then assume that the effective amplitude in Eq. (2) arises at one loop by the exchange inside the loop of dark and messenger fields, the latter being charged under both SM and extra $U(1)_F$ gauge interactions. By naive dimensional analysis, one expects the $\Lambda_{\gamma\bar{\gamma}}$ scale to be proportional to the mass of the heaviest particle running in the loop, presumably related to the dark sector. If this were the case, the chances of observing this process at the LHC would be dramatically limited to a light dark-sector scenario, which is a quite strong requirement. On the contrary, due to the nondecoupling properties of the Higgs boson, this scale could be proportional to the Higgs vacuum expectation value (VEV) (similarly to what happens for the $H \to \gamma\gamma$, γZ, gg decay rates), which would allow for potentially large rates regardless of the characteristic mass scale of the dark sector. This crucial property turns out to hold in the framework of the model proposed in Ref. [14], as has been explicitly verified in Ref. [15]. This framework can then be used as a benchmark model for computing all the relevant quantities for predicting the Higgs decay rates into dark photons.

In Ref. [14], the flavor and chiral symmetry breaking (ChSB) were assumed to be generated in a dark sector, and transferred to the Higgs Yukawa sector at one loop via Higgs-portal type scalar-messenger fields. A new exact $U(1)_F$ gauge symmetry in the dark sector produces via a nonperturbative mechanism an exponential spread in the Yukawa couplings Y_i (with i a flavor index), providing a natural solution to the SM flavor hierarchy problem. Apart from the gauge boson of the unbroken $U(1)_F$ gauge group (the massless dark photon), the dark sector consists of SM-singlet massive dark fermions, Q_i, a sort of rescaled replica

of SM fermions. The requirement that the gauge sector is unbroken allows dark fermions, which have $U(1)_F$ charges, to be stable and thus potential dark-matter candidates. In addition to the dark sector, there are scalar messenger fields (with the same quantum numbers as the squarks and sleptons of supersymmetric models), which communicate the ChSB and flavor breaking from the dark sector to the Yukawa couplings.

By restricting, for instance, only to the contribution of colored messenger fields, the effective $\Lambda_{\gamma\bar{\gamma}}$ scale can then be exactly derived in the low-energy limit [15]. In particular, for a universal average messenger mass $\bar{m}$, one obtains [up to corrections of order $o(m_H^2/\bar{m}^2)$]

$$\frac{1}{\Lambda_{\gamma\bar{\gamma}}} = \frac{R\sqrt{\alpha\bar{\alpha}}}{6\pi v}\frac{\xi^2}{1-\xi^2}, \tag{4}$$

where v is the Higgs VEV, $R = N_c \sum_{i=1}^{3} (e_U q_{U_i} + e_D q_{D_i})$, where q_{U_i}, q_{D_i} are the $U(1)_F$ charges in the up and down sectors, $e_U = \frac{2}{3}$, $e_D = -\frac{1}{3}$ are the corresponding EM charges, α is the EM fine-structure constant, and $N_c = 3$ is the number of colors. Also, $\xi = \Delta/\bar{m}^2$, with $\Delta = \mu_S v$ parametrizing the left-right mixing of the messengers scalars, and μ_S is the VEV of a singlet scalar field. The latter spontaneously breaks the $H \to -H$ parity symmetry needed to forbid Higgs Yukawa interactions at tree level, since Yukawa couplings are generated radiatively [14].

The nondecoupling properties of the Higgs boson clearly show up in Eq. (4). Indeed, the effective $\Lambda_{\gamma\bar{\gamma}}$ scale turns out to be proportional to the Higgs VEV, that is it tends to a finite value in the limit $\bar{m} \to \infty$ (for fixed mixing parameter $\xi < 1$). As stressed in Ref. [15], this is a general property of the Higgs boson, and does not depend on the peculiar structure of the model in Ref. [14], provided a messenger sector letting the SM and the dark sector communicate exists.

The same off-shell fields contributing to the $H \to \gamma\bar{\gamma}$ decay amplitude at one loop can also induce the $H \to \bar{\gamma}\bar{\gamma}$ transition to two dark photons, increasing the invisible Higgs decay width. The projected sensitivity of the high-luminosity LHC for the invisible branching ratio of the Higgs is at the 10% level [17,18]. Additionally, extra contributions to the $H \to \gamma\gamma$, γZ, gg SM decay rates can be expected. By parametrizing these effects in a model-independent way, $\mathrm{BR}_{\gamma\bar{\gamma}}$ values up to 5% can be allowed, while respecting all other LHC constraints [15]. Such large BR values for $H \to \gamma\bar{\gamma}$ are natural in the framework of the model in Ref. [14] (see also Ref. [19] for more model-dependent predictions).

Such high decay rates strongly motivated the study of the Higgs production followed by the $H \to \gamma\bar{\gamma}$ decay at the LHC Run-1 energy and integrated luminosity [15]. The corresponding signature is indeed quite distinctive, with an almost monochromatic and massless invisible (dark-photon) system and equally monochromatic photon, jointly resonating at the Higgs mass.

In the present study, we will extend our previous analysis to the 14 TeV LHC setup, upgrading different aspects of the study of the main gluon-fusion production channel, and including VBF Higgs production in order to improve the final sensitivity to the $H \to \gamma\bar{\gamma}$ signature.

III. PHENOMENOLOGICAL ANALYSIS

A. Gluon-fusion channel

We start by extending our previous LHC analysis of the gluon-fusion process at 8 TeV [15] to 14 TeV, improving the treatment of both the signal and the main SM backgrounds. A crucial point in the refinement of most important backgrounds will be the use of recently published experimental data by the CMS Collaboration [16], where the relevant SM backgrounds are measured and reported. We will model our background accordingly. All this will result in a higher reliability of our signal and background estimates, that will anyhow substantially confirm our previous results on discovery potential based on a more *naive* analysis.

The process $pp \to H \to \gamma\bar{\gamma}$, where the Higgs is produced in the gluon-fusion channel, is characterized by a single photon recoiling against missing transverse momentum. In our previous analysis we outlined a search strategy for this process, based on the following requirements (now slightly updated to take into account smearing effects discussed in the following):

(i) one isolated ($\Delta R > 0.4$) photon with $p_T^\gamma > 50$ GeV, and $|\eta^\gamma| < 1.44$;
(ii) missing transverse momentum satisfying $\not{E}_T > 50$ GeV;
(iii) transverse mass in the range $100\ \mathrm{GeV} < M_{\gamma\bar{\gamma}}^T < 130\ \mathrm{GeV}$;
(iv) no isolated leptons.

The transverse-mass variable is defined as $M_{\gamma\bar{\gamma}}^T = \sqrt{2p_T^\gamma \not{E}_T(1-\cos\Delta\phi)}$, where $\Delta\phi$ is the azimuthal distance between the photon transverse momentum p_T^γ, and the missing transverse momentum $\not{E}_T$.

The main SM background for the above selection criteria is $pp \to \gamma j$, where the missing transverse momentum can arise from a) neutrinos following heavy-flavor decays in the jet, b) mismeasurement of the jet energy, and c) very forward particles escaping the detector. $pp \to jj$ also contributes to the latter channel, whenever one of the jets is misidentified as a photon. We assume the corresponding mistagging probability to be 0.1%. Also, a photon identification efficiency of 90% is adopted throughout this analysis. In our previous study [15], the hadronic SM background was estimated at parton level in a quite crude way, by treating any parton with $|\eta| > 4.0$ as missing energy.

The CMS analysis of the data set at 8 TeV in Ref. [16] assumes event selection criteria quite similar to the above, in order to search for an exotic three-body decay of the

Higgs boson into a photon and two invisible particles. Unfortunately, the CMS analysis imposes an upper limit of 60 GeV on the photon transverse momentum, cutting away an important fraction of the signal region for the two-body decay of interest here (for which $p_T^\gamma \lesssim m_H/2$). However, due to the similarity of the residual event selection criteria in the two analyses, the continuous SM backgrounds are expected to be comparable. As a consequence, we decided to model our QCD background according to the CMS measured distributions, benefitting from the highly optimized experimental procedure for the missing transverse-momentum determination. This will lead to a much improved reliability of our background estimate in the gluon-fusion channel.

We started by simulating the γj and dijet backgrounds with MadGraph5_aMC@NLO (v2.2.2) [20], interfaced with PYTHIA (v6.4.28)[21], hence including initial- and final-state radiation (ISR and FSR), hadronization and detector-resolution effects in the present updated analysis. We have generated event samples both at 8 and 14 TeV. We have then matched our 8 TeV samples to the event yield corresponding to the "*SUSY benchmark*" event selection criteria reported in the CMS analysis [16]. This matching results in k factors connecting our simulated samples to experimental data at 8 TeV. We find $k = 0.11$ for the γj background, and $k = 0.058$ for the $j \to \gamma$ background. The order-of-magnitude reduction in the background estimate reported by CMS as compared to our simulation is to be understood as a result of CMS's advanced strategies for reducing event yields arising from mismeasured missing transverse momentum in hadronic events, as detailed in Ref. [16]. It is beyond the scope of this work to attempt to exactly reproduce the CMS analysis. Instead, we assume that the CMS optimization strategy works with comparable efficiency also in 14 TeV collisions, and that the corresponding reduction of the 14 TeV hadronic SM backgrounds is reliably captured by rescaling our simulated samples with the same k factors obtained from the 8 TeV matching.

We also upgraded the simulation of $H \to \gamma\bar{\gamma}$ signal events by including the ISR effects. Accordingly, we simulated Higgs production in association with either one or no jets with ALPGEN (v2.14) [22], interfaced with PYTHIA for jet-parton matching, hadronization and detector-resolution effects (see Sec. III B for the jet definition and other simulation details).

The corresponding smearing in the p_T^γ and $M_{\gamma\bar{\gamma}}^T$ spectra for the $H \to \gamma\bar{\gamma}$ signal is shown in Fig. 1. There, the two categories corresponding to no extra jets and one extra jet accompanying the Higgs signal are shown separately, along with the distributions for the hadronic backgrounds coming from γj production, and dijet production followed by $j \to \gamma$ mistagging. The latter distributions are obtained with a nominal cut on the photon transverse momentum, $p_T^\gamma > 10$ GeV, and $p_T^j > 10$ GeV on fake jets in the dijet analysis.

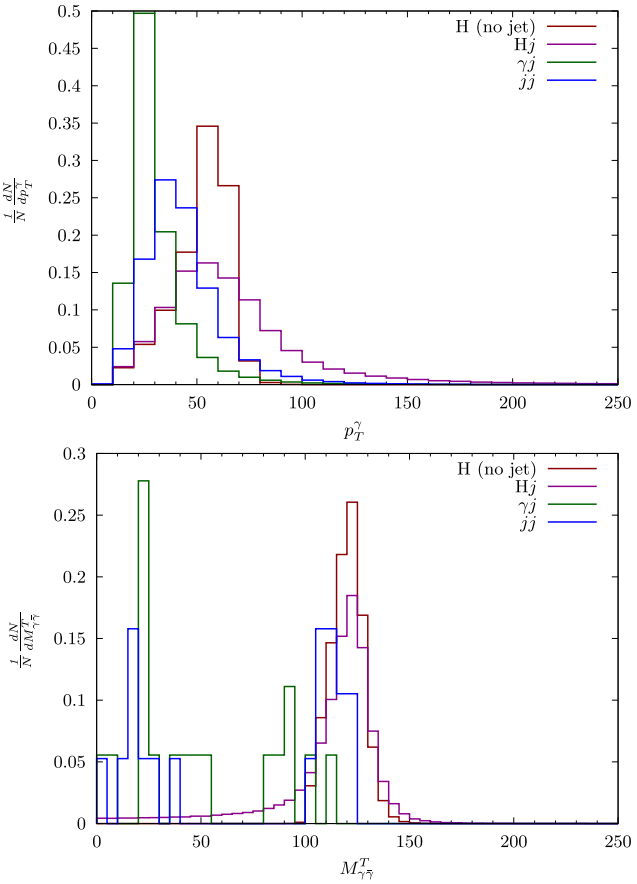

FIG. 1. Photon p_T (upper plot) and transverse-mass (lower plot) distributions for the $H \to \gamma\bar{\gamma}$ signal in the gluon-fusion process, and for SM backgrounds, for inclusive $\gamma + \not{E}_T$ final states with no isolated leptons. The effect of extra radiation on the signal events is also depicted. All distributions are normalized to unity.

Because of initial-state-radiation and detector-resolution effects, a better sensitivity for the signal is obtained by relaxing the maximum value of the photon transverse-momentum cut, and increasing the transverse mass window from 100 GeV $< M_{\gamma\bar{\gamma}}^T <$ 126 GeV to 100 GeV $< M_{\gamma\bar{\gamma}}^T <$ 130 GeV with respect to Ref. [15].

The main electroweak background consists of the channels $pp \to W \to e\nu$, where the electron is misidentified as a photon, $pp \to W(\to \ell\nu)\gamma$, for ℓ outside charged-lepton acceptance, and $pp \to Z(\to \nu\nu)\gamma$. We have simulated these processes at parton level according to the analysis in Ref. [15], using a $e \to \gamma$ conversion probability of 0.005 for the first process.

In Table I, one can find a summary of the cross sections times acceptance (in fb) for the signal and backgrounds at 8 and 14 TeV for the gluon-fusion process, assuming $\mathrm{BR}_{\gamma\bar{\gamma}} = 1\%$, and obtained as discussed above.

With the 20 fb^{-1} data set at 8 TeV, our improved analysis gives a 5σ discovery reach at $\mathrm{BR}_{\gamma\bar{\gamma}} \simeq 4.8 \times 10^{-3}$, compatible with our previous estimate [15]. The present more realistic event simulation was expected to deteriorate the

TABLE I. Cross section times acceptance A (in fb) for the gluon-fusion signal and backgrounds at 8 and 14 TeV, assuming $\mathrm{BR}_{\gamma\bar{\gamma}} = 1\%$, with the selection $p_T^\gamma > 50$ GeV, $|\eta^\gamma| < 1.44$, $\not{E}_T > 50$ GeV, and 100 GeV $< M_{\gamma\bar{\gamma}}^T < 130$ GeV.

	$\sigma \times A$ [8 TeV]	$\sigma \times A$ [14 TeV]
$H \to \gamma\bar{\gamma}$ ($\mathrm{BR}_{\gamma\bar{\gamma}} = 1\%$)	44	101
γj	63	202
$jj \to \gamma j$	59	432
$e \to \gamma$	55	93
$W(\to \ell\nu)\gamma$	58	123
$Z(\to \nu\nu)\gamma$	102	174
total background	337	1024

capability of separating signal from background. This effect has been actually mostly compensated by the advanced optimization experimental strategies recently applied to the missing transverse-momentum data, on which we have now modeled our background simulation.

Assuming an integrated luminosity of 100 (300) fb^{-1} at 14 TeV, and extrapolating the effect of these optimization techniques to higher energies, we find a 5σ discovery potential for $\mathrm{BR}_{\gamma\bar{\gamma}}$ down to $1.6 \times 10^{-3} (9.2 \times 10^{-4})$. At the High-Luminosity LHC (HL-LHC), with an integrated luminosity of 3 ab^{-1}, the 5σ reach is extended down to 2.9×10^{-4}.

B. VBF channel

We now turn our focus to the Higgs production in the VBF channel. This presents a lower production rate with respect to the gluon-fusion channel. On the other hand, it is in principle more controllable due to its strong kinematical characterization. In particular, the process $pp \to Hjj \to \gamma\bar{\gamma}jj$, where the Higgs boson arises from a $W(Z)$-pair fusion, results mostly in two forward jets with opposite rapidity, one photon and missing transverse momentum.

We started by simulating the signal with PYTHIA, by including both the Higgs VBF production and its subsequent decay into a $\gamma\bar{\gamma}$ final state. The main SM backgrounds are given by the production of QCD multijets, $\gamma +$ jets, and $\gamma + Z(\to \bar{\nu}\nu) +$ jets. The $\gamma +$ jets background has been simulated using ALPGEN. We have generated γj, γjj, and γjjj samples with $p_T^\gamma > 10$ GeV and $|\eta^\gamma| < 2.5$ for photons, and $p_T^j > 20$ GeV and $|\eta^j| < 5$ for jets. An isolation of $\Delta R > 0.4$ between all pairs of objects is required. We have then interfaced ALPGEN and PYTHIA, and incorporated the jet-parton matching, according to the MLM prescription as defined in Ref. [23]. Events containing hard partons are generated in ALPGEN with a cut on the transverse momentum ($p_T > 20$ GeV), and on the rapidity ($|\eta| < 5.0$) of each parton, along with a minimum separation ($\Delta R > 0.4$) between them. These events are then interfaced with PYTHIA for showering, to take into account soft and collinear emission of partons. All partons are then clustered using a cone jet algorithm with $p_T > 20$ GeV, and a cone size of $\Delta R = 0.6$ (the latter used only for matching purposes, not for the jet definition in the event selection). An event is said to be matched if there is a one-to-one correspondence between jets and initial hard partons. An event with an extra jet which is not matched to a parton is rejected in case of exclusive matching, while it is kept in case of inclusive matching for the highest jet-multiplicity samples.

For the QCD multijet process and the $\gamma + Z +$ jets process we have used MadGraph 5 interfaced with PYTHIA. In the case of the QCD multijet process, the most central jet is assumed to be mistagged as a photon with a corresponding faking probability of 0.1%. The ISR and FSR effects, parton shower, hadronization and finite detector resolution effects have also been implemented for the signal and all backgrounds. We have then assumed a photon identification efficiency of 90%. The distributions are obtained with a nominal cut on the photon transverse momentum, $p_T^\gamma > 10$ GeV, and $p_T^j > 10$ GeV on fake jets in the QCD multijet analysis.

In Figs. 2 and 3, we plot a few kinematic distributions which are useful to separate the signal from the backgrounds.

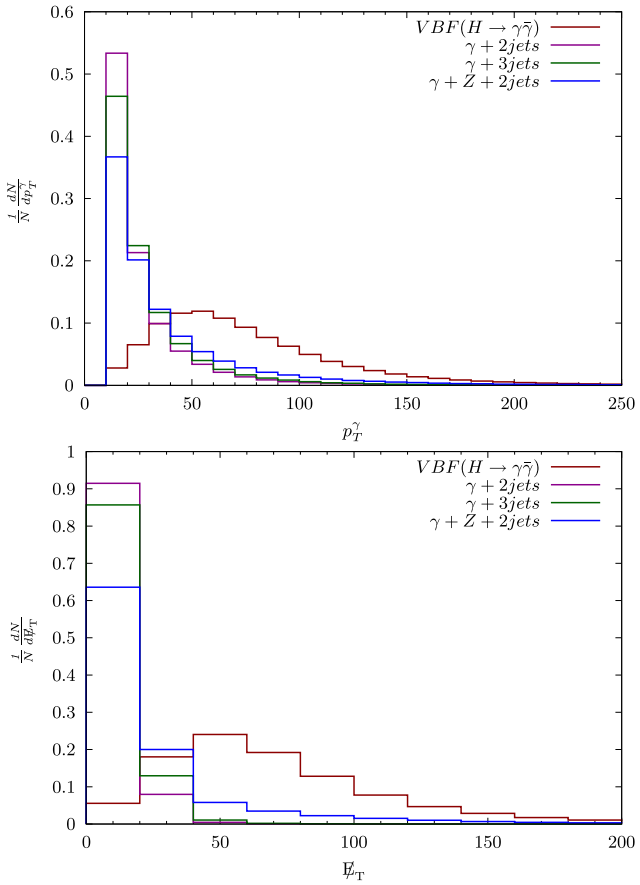

FIG. 2. Photon p_T (upper plot), and missing transverse-energy (lower plot) distributions for the signal and SM backgrounds in the VBF process. The final state in this case is $\gamma + \not{E}_T + (\geq 2)$ jets with no isolated leptons. All distributions are normalized to unity.

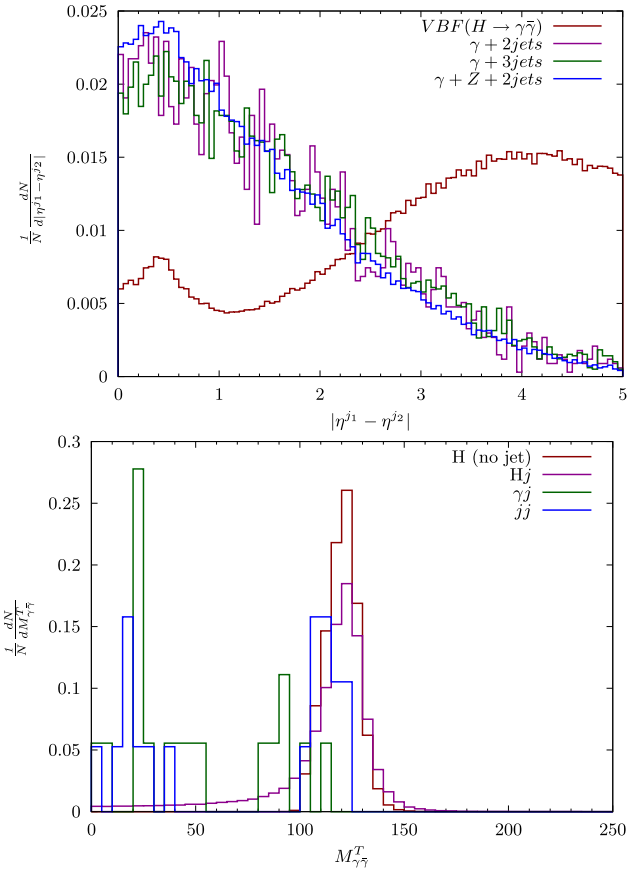

FIG. 3. Rapidity gap between the two forward jets (upper plot), and transverse-mass (lower plot) distributions for the signal and SM backgrounds in the $\gamma + \not{E}_T + (\geq 2)$ jets final state with no isolated leptons. The $\Delta\eta = |\eta^{j_1} - \eta^{j_2}|$ distribution is obtained with a cut $p_T^\gamma > 30$ GeV, for $p_T^j > 30$ GeV on the fake jet in the QCD multijet analysis, and $\not{E}_T > 30$ GeV. The transverse mass distribution is obtained with the additional cuts $\eta^{j_1} \times \eta^{j_2} < 0$ and $|\eta^{j_1} - \eta^{j_2}| > 4.0$. All distributions are normalized to unity.

On this basis, we propose to select the events according to the following criteria:

(i) (*basic cuts*) one isolated photon with $p_T^\gamma > 30$ GeV and $|\eta^\gamma| < 2.5$, and two or more jets with $p_T^j > 20$ GeV and $|\eta^j| < 5.0$, and angular separation $\Delta R > 0.4$ between all objects;
(ii) (*basic cut*) missing transverse energy $\not{E}_T > 30$ GeV;
(iii) (*basic cut*) no isolated leptons;
(iv) (*rapidity cuts*) rapidities of the two highest-p_T jets obey $\eta^{j_1} \times \eta^{j_2} < 0$ and $|\eta^{j_1} - \eta^{j_2}| > 4.0$;
(v) ($M^T_{\gamma\bar{\gamma}}$ *cuts*) transverse mass of the photon and invisible system satisfying 100 GeV $< M^T_{\gamma\bar{\gamma}} <$ 130 GeV (as above, the upper bound has been extended with respect to m_H to take into account the smearing of the $M^T_{\gamma\bar{\gamma}}$ distribution, cf. Fig. 3).

In Table II, we present the cross sections for the signal and dominant SM backgrounds after the sequential application of basic cuts, rapidity cuts on the two forward jets, and transverse-mass cut on the photon plus missing transverse-energy system.

TABLE II. Cross sections times acceptance $\sigma \times A$ (in fb) for the VBF signal and backgrounds at 14 TeV, after sequential application of cuts defined in the text, assuming $\mathrm{BR}_{\gamma\bar{\gamma}} = 1\%$.

Cuts	Signal	γ + jets	$\gamma + Z$ + jets	QCD multijet
Basic cuts	17.7	266636	1211	72219
Rapidity cuts	8.8	8130	38.1	33022
$M^T_{\gamma\bar{\gamma}}$ cuts	5.0	574	6.5	3236

In order to better control the missing transverse energy arising from jet energy mismeasurements, we have also imposed an azimuthal isolation cut $\Delta\phi(j_i, \not{E}_T) > 1.5$ (with $i = 1, 2$) on the angles between the $\not{E}_T$ direction and the transverse momenta of the two highest-p_T jets.

Furthermore, we studied the effect of a selection cut occasionally applied for searches in the VBF channel (see, e.g., the $W \to \ell\nu$ analysis in VBF in Ref. [24]). This is the $y^* < 1.0$ cut on the Zeppenfeld variable defined as $y^* = |y^H - \frac{1}{2}(\eta^{j_1} - \eta^{j_2})|$, where the Higgs rapidity y^H is reconstructed from the photon momentum and the missing transverse energy as described in Ref. [25]. X systems produced via VBF are in fact characterized by a smaller y^* value, with respect to other X + 2-jet backgrounds. The values of the $\Delta\phi(j_i, \not{E}_T)$ and y^* cuts have been separately optimized in order to increase the signal significance.

Table III presents the independent effect of the y^* and $\Delta\phi(j_i, \not{E}_T)$ cuts, applied after the set of cuts listed in Table II. The combined effect of these two cuts is also shown in the last row of Table III. The $\Delta\phi(j_i, \not{E}_T)$ cut turns out to be much more effective in separating the signal from background. We then dropped the y^* cut in our final selection.

Since the $\Delta\phi(j_i, \not{E}_T)$ distribution is asymmetric in the exchange of the first and second highest-p_T jets, we have also tried to optimize the signal significance by assuming an asymmetric cut on $\Delta\phi(j_i, \not{E}_T)$, that is by applying different cuts on the first and second highest-p_T jets. We anyway found that the best signal-to-background ratio is

TABLE III. Cross sections times acceptance $\sigma \times A$ (in fb) for the VBF signal and backgrounds at 14 TeV, assuming $\mathrm{BR}_{\gamma\bar{\gamma}} = 1\%$. The first and second rows correspond to the separate effect of the y^* and $\Delta\phi(j_i, \not{E}_T)$ cuts, respectively, after applying the cut sequence in Table II. The last row represents the combined effects of the two cuts. The last column shows the signal significance for an integrated luminosity of $\mathrm{L} = 300$ fb^{-1}.

Cuts	Signal	γ + jets	$\gamma + Z$ + jets	Multijet	$\mathrm{L} = 300$ fb^{-1}
$y^* < 1.0$	2.67	84.2	1.84	758	1.6σ
$\Delta\phi(j_i, \not{E}_T) > 1.5$	1.82	6.9	2.16	37	4.6σ
Both cuts	1.21	1.2	0.67	19	4.5σ

obtained with the symmetric cut $\Delta\phi(j_i, \not{E}_T) > 1.5$ on both jets.

Finally, assuming an integrated luminosity of 300 fb^{-1}, in the last column of Table III we present the estimated VBF signal significances for $\mathrm{BR}_{\gamma\bar{\gamma}} = 1\%$. For this setup, the signal significance $S/\sqrt{S+B}$ approaches the 5σ level. For 100 fb^{-1}, the 5σ reach in the branching ratio is about $\mathrm{BR}_{\gamma\bar{\gamma}} \simeq 2\%$. With the HL-LHC integrated luminosity of 3 ab^{-1}, the 5σ reach can be extended down to $\mathrm{BR}_{\gamma\bar{\gamma}} = 3.4 \times 10^{-3}$.

IV. SUMMARY AND CONCLUSIONS

We have studied the prospects for discovering an exotic Higgs-boson decay into a SM photon and a new neutral massless vector boson, a dark photon, at the LHC with $\sqrt{S} = 14$ TeV. We have updated our previous analysis of the gluon-fusion channel at 8 TeV by a more reliable treatment of both the signal and hadronic SM backgrounds, and extended this approach to 14 TeV collisions. We also explored for the first time the possibility of detecting the exotic $H \to \gamma\bar{\gamma}$ channel in the VBF Higgs production.

A summary of our findings is presented in Table IV, where we show the predicted reach in detectable $\mathrm{BR}_{\gamma\bar{\gamma}}$ for both exclusion (at a 3σ level) and discovery (at a 5σ level), assuming 100, 300 and 3000 fb^{-1} of data at 14 TeV. The gluon-fusion potential turns out to be definitely higher, extending the $\mathrm{BR}_{\gamma\bar{\gamma}}$ reach with respect to the VBF channel by more than 1 order of magnitude. In particular, according to the present analysis, the full LHC program will allow us to discover (exclude) a $\mathrm{BR}_{\gamma\bar{\gamma}}$ value down to less than $1 \times 10^{-3} (6 \times 10^{-4})$, while the HL-LHC phase will be sensitive to $\mathrm{BR}_{\gamma\bar{\gamma}}$ as small as $3 \times 10^{-4} (2 \times 10^{-4})$. We recall that $\mathrm{BR}_{\gamma\bar{\gamma}}$ values up to 5% are allowed in realistic beyond-the-SM frameworks [15].

In light of the projected discovery reach and of the theoretical interest in dark-photon models, we urge the ATLAS and CMS experiments to perform a dedicated analysis of the $H \to \gamma + \not{E}_T$ signature in two-body final states. The event selection criteria used in the CMS analysis [16], by imposing an upper limit of 60 GeV on p_T^γ, considerably restrict the signal phase space for the two-body decay mode. Nevertheless, the methods used by CMS for the suppression of the SM hadronic backgrounds to the $\not{E}_T$ signature can be very effective even for relatively low transverse-momentum final states, possibly resulting in experimental sensitivities for branching ratios well below the per mil level. Similar methods could actually be applied (once the corresponding experimental analyses will be available) for suppressing the SM multijet background to the VBF channel, possibly increasing the relative weight of the VBF analysis in the search for a $H \to \gamma\bar{\gamma}$ signature, and hence expanding the LHC potential.

TABLE IV. Reach in $\mathrm{BR}_{\gamma\bar{\gamma}}$ (in percentage) for a 3σ exclusion or a 5σ discovery at the 14 TeV LHC, in the VBF and gluon-fusion channels, for different integrated luminosities L.

$\mathrm{BR}_{\gamma\bar{\gamma}}$ (%)	L = 100 fb^{-1}		L = 300 fb^{-1}		L = 3 ab^{-1}	
Significance	3σ	5σ	3σ	5σ	3σ	5σ
$\mathrm{Br}_{\gamma\bar{\gamma}}$(VBF)	1.1	1.9	0.65	1.1	0.21	0.34
$\mathrm{Br}_{\gamma\bar{\gamma}}(ggF)$	0.096	0.16	0.055	0.092	0.017	0.029

After the recent observation at the LHC of an excess in the diphoton spectrum around an invariant mass of about 750 GeV [26,27], it would also be advisable to extend the search for $\gamma + \not{E}_T$ final states to higher invariant masses of the $\gamma\bar{\gamma}$ pair. Indeed, the observed features of the would-be 750 GeV $\gamma\gamma$ resonance might require new degrees of freedom in a hidden sector in order to give rise to effective couplings to photons (and gluons) (see, e.g., Ref. [28]). The latter degrees of freedom could well be portals to a massless dark photon, in case they are also charged under an extra unbroken $U(1)_F$. Since a large $U(1)_F$ coupling might be naturally allowed [19], the corresponding rate for a $\gamma\bar{\gamma}$ resonance at 750 GeV could already be sizable with the present data set. This possibility has also been envisaged in Refs. [29–31].

In case the diphoton signature is confirmed at the LHC, the search for new structures in the $\gamma + \not{E}_T$ transverse-mass distributions at 750 GeV would provide extra invaluable insight about the nature of the NP behind it.

ACKNOWLEDGMENTS

We thank Daniel Fournier, Jean-Baptiste de Vivie de Régie, and Rachid Mazini for useful discussions. E. G. would like to thank the TH division of CERN for its kind hospitality during the preparation of this work. The work of M. H. has been supported by the Academy of Finland Project No. 267842.

[1] P. Ade *et al.* (Planck Collaboration), Astron. Astrophys. **571**, A16 (2014).
[2] For a review and references see, R. Essig *et al.*, arXiv: 1311.0029.
[3] B. Holdom, Phys. Lett. **166B**, 196 (1986).
[4] S. Chatrchyan *et al.* (CMS Collaboration), Phys. Rev. Lett. **108**, 261803 (2012); G. Aad *et al.* (ATLAS Collaboration), Phys. Rev. Lett. **110** (2013) 011802.

[5] G. Aad *et al.* (ATLAS Collaboration), Phys. Rev. D **87**, 112003 (2013); S. Chatrchyan *et al.* (CMS Collaboration), J. High Energy Phys. 10 (2013) 164.
[6] D. Curtin *et al.*, Phys. Rev. D **90**, 075004 (2014); J. F. Kamenik and C. Smith, Phys. Rev. D **85**, 093017 (2012); H. Davoudiasl, H.-S. Lee, I. Lewis, and W. J. Marciano, Phys. Rev. D **88**, 015022 (2013); Y. Sun and D.-N. Gao, Phys. Rev. D **89**, 017301 (2014).
[7] A. Falkowski and R. Vega-Morales, J. High Energy Phys. 12 (2014) 037.
[8] L. Ackerman, M. R. Buckley, S. M. Carroll, and M. Kamionkowski, Phys. Rev. D **79**, 023519 (2009).
[9] J. Fan, A. Katz, L. Randall, and M. Reece, Phys. Rev. Lett. **110**, 211302 (2013).
[10] M. Heikinheimo, M. Raidal, C. Spethmann, and H. Veerme, Phys. Lett. B **749**, 236 (2015).
[11] N. Arkani-Hamed, D. P. Finkbeiner, T. R. Slatyer, and N. Weiner, Phys. Rev. D **79**, 015014 (2009).
[12] K. M. Zurek, Phys. Rep. **537**, 91 (2014).
[13] H. An, M. Pospelov, J. Pradler, and A. Ritz, Phys. Lett. B **747**, 331 (2015).
[14] E. Gabrielli and M. Raidal, Phys. Rev. D **89**, 015008 (2014).
[15] E. Gabrielli, M. Heikinheimo, B. Mele, and M. Raidal, Phys. Rev. D **90**, 055032 (2014).
[16] V. Khachatryan *et al.* (CMS Collaboration), Phys. Lett. B **753**, 363 (2016).
[17] H. Okawa, J. Kunkle, and E. Lipeles, arXiv:1309.7925.
[18] S. Dawson *et al.*, arXiv:1310.8361.
[19] S. Biswas, E. Gabrielli, M. Heikinheimo, and B. Mele, J. High Energy Phys. 06 (2015) 102.
[20] J. Alwall, R. Frederix, S. Frixione, V. Hirschi, F. Maltoni, O. Mattelaer, H.-S. Shao, T. Stelzer, P. Torrielli, and M. Zaro, J. High Energy Phys. 07 (2014) 079.
[21] T. Sjostrand, S. Mrenna, and P. Z. Skands, J. High Energy Phys. 05 (2006) 026.
[22] M. L. Mangano, M. Moretti, F. Piccinini, R. Pittau, and A. D. Polosa, J. High Energy Phys. 07 (2003) 001.
[23] S. Hoeche, F. Krauss, N. Lavesson, L. Lonnblad, M. Mangano, A. Schalicke, and S. Schumann, arXiv:hep-ph/0602031.
[24] CMS Collaboration, Report No. CMS-PAS-SMP-13-012.
[25] D. L. Rainwater, R. Szalapski, and D. Zeppenfeld, Phys. Rev. D **54**, 6680 (1996).
[26] ATLAS Collaboration, Report No. ATLAS-CONF-2015-081.
[27] CMS Collaboration, Report No. CMS-PAS-EXO-15-004.
[28] R. Franceschini, G. F. Giudice, J. F. Kamenik, M. McCullough, A. Pomarol, R. Rattazzi, M. Redi, F. Riva, A. Strumia, and R. Torre, J. High Energy Phys. 03 (2016) 144.
[29] X. J. Bi, Z. Kang, P. Ko, J. Li, and T. Li, arXiv:1602.08816.
[30] Y. Tsai, L. T. Wang, and Y. Zhao, arXiv:1603.00024.
[31] C. Y. Chen, M. Lefebvre, M. Pospelov, and Y. M. Zhong, arXiv:1603.01256.